Optimal Joint Access Point Placement and Resource Allocation for Indoor mmWave Communications

Ozan Alp Topal*, Emil Björnson*, Dominic Schupke† and Cicek Cavdar*
* School of Electrical Engineering and Computer Science, KTH Royal Institute of Technology, Stockholm, Sweden
† Airbus, Central Research and Technology, Munich, Germany,
E-mail: *{oatopal, emilbjo, cavdar}@kth.se, †dominic.schupke@airbus.com

***Abstract*—In this paper, we formulate and solve the optimization problem for joint access point placement and resource allocation for indoor mmWave communications with static users, with a particular focus on airplanes. The proposed scheme obtains the required number of access points (APs) and their locations, for a given data rate threshold and given radio resources such as bandwidth, antenna numbers, and AP cooperation. We first build an airplane cabin environment in a ray-tracing tool to realistically capture the propagation effects. Then, we cast optimal deployment problems considering the performance of different AP cooperation schemes, namely coordinated scheduling (CS), non-coherent joint transmission (NC-JT), and coherent joint transmission (C-JT). The results indicate that full cooperation among the APs with C-JT requires fewer APs, especially under high data rate requirements. Comparing the network deployments in the mmWave and sub-6GHz bands, we observe 9 times higher data rates in mmWave although more APs are required.**

***Index Terms*—Millimeter wave communications, radio resource allocation, access point deployment, ray-tracing.**

I. Introduction

With emerging applications such as ultra-high definition video streaming, virtual reality (VR), and wireless cognition, the demand for mobile network data is expected to grow in the 6G networks [1]. To support the high demand, the millimeter wave (mmWave) bands (24-78 GHz) are promising due to the large amount of available bandwidth. Despite this advantage, mmWave communication is more sensitive to variations in the propagation environment and blocking of individual propagation paths compared to the conventional sub-6-GHz bands [2]. One method to improve the signal quality is beamforming, where multi-antennas at the access point (AP) side focus the radiated energy towards the receiver to extend coverage [2]. Another method is the cooperation among several APs to have a macro diversity if one AP link is blocked [3]. Since the service quality is largely affected by the environment geometry and the blocking objects, the correct positioning of the APs is a necessary step to guarantee the best performance with fewer radio elements.

There are several prior works on mmWave network deployment, whereof most focus on outdoor environments, where the users are mobile, and expanding the coverage area is the main objective of the deployment [4], [5]. In [4], the coverage area is maximized by increasing the availability of line-of-sight (LOS) links. The authors aim at providing desired received signal power levels over randomly generated city maps [5]. The mmWave network deployment is less investigated for indoor environments than the outdoors. The authors of [6] focus on maximizing the LOS coverage probability for indoor mmWave networks. In [7], the authors solve optimal user association and AP deployment jointly for indoor mmWave networks. The coverage is defined on a grid basis, where users are mobile and randomly distributed over a single grid. Although these works guarantee a certain signal strength or link availability, they do not consider the effect of radio resource allocation (bandwidth/time/power) and the number of users in the environment.

To consider these effects, one can start by investigating user environments that are structured and - during the main network operation - essentially static, i.e. no drastic changes in the propagation conditions are expected. Public transportation vehicles, e.g., buses, trains, and airplanes are examples of such indoor dense spaces (IDS), since users are mainly sitting on their seats, which is also the time where their communication demand tends to increase [8]. In such environments, minimizing the number of deployed APs is essential, since it reduces overall hardware cost, efforts in wiring APs during installation, and weight. One can benefit by considering the available radio resources such as bandwidth, time, access point cooperation, power, and antenna limits of the access points as part of the AP deployment problem to further reduce the number of deployed APs. For example, if a certain user location is disadvantageous because of a blockage, instead of deploying more APs to provide higher signal-to-noise (SNR) ratio, we can assign more time/frequency resources to satisfy the rate requirement of the user.

In this case, the following question can be raised: "How much can we minimize the number of required APs by optimizing the allocation of radio resources jointly?" To answer this question, the main contributions of this work are as follows:

- We formulate and solve an optimal AP deployment problem that minimizes the number of APs and jointly allocates time proportions to users while guaranteeing the

Results incorporated in this paper received funding from the ECSEL Joint Undertaking (JU) under grant agreement No 876124. The JU receives support from the EU Horizon 2020 research and innovation programme and Vinnova in Sweden.

rate requirement of each user.

- We consider three levels of AP cooperation, namely cooperated scheduling (CS), non-coherent joint transmission (NC-JT), and coherent joint transmission (C-JT), and derive mixed-binary programming forms for each problem, which can be optimally solved.
- As a case study, we build a realistic airplane cabin environment using a commercial ray-tracing (RT) program to obtain channel coefficients in the 28 GHz and 2.4 GHz bands. Through numerical analysis, we demonstrate the performance gains by AP cooperation, the usefulness of our optimization solutions, and the main limiting factors.

II. System Model

We consider the downlink transmission in a mmWave MIMO system comprised of a set of APs, $\mathcal{B}_a = \{B_1^a, B_2^a, \ldots, B_{L_a}^a\}$, and a fixed set of static user equipments (UEs) $\mathcal{U} = \{U_1, U_2, \ldots, U_K\}$ in an indoor area. The optimal AP locations are selected from a finite set of candidate AP locations, $\mathcal{B} = \{B_1, B_2, \ldots, B_L\}$, where $|\mathcal{B}| = L$ and $\mathcal{B}_a \subseteq \mathcal{B}$. The APs and UEs are respectively equipped with n_t and n_r antenna elements. We consider an interference-free multiple access scenario, where the UEs are scheduled over orthogonal time resources. The time proportion of the kth UE is denoted by τ_k, and $\sum_{k=1}^{K} \tau_k = 1$. Considering coding over long blocklengths, the achievable data rate of the kth UE is

$$R_k = \tau_k W \log_2(1 + \mathrm{SNR}_k), \tag{1}$$

where W is the total bandwidth and SNR_k is the SNR. We consider CS, NC-JT, and C-JT as three different levels of cooperation strategies among APs. While a single AP serves a single UE at a given time proportion in CS, in NC-JT and C-JT, the APs jointly serve to a single UE. In C-JT, the APs are able to simultaneously transmit the same message signal to the selected UE phase-coherently, whereas in NC-JT, the APs transmit independent data streams to the UE. Regardless of the cooperation strategy, the transmitted message signal from the AP l for the UE k is denoted by

$$\mathbf{x}_{kl} = \sqrt{q_{kl}} \mathbf{w}_{kl} \zeta_{kl} \in \mathbb{C}^{n_t}, \tag{2}$$

where $l \in \mathcal{B}_k$ and $k = \{1, 2, \ldots, K\}$. $\mathcal{B}_k$ denotes the set of serving APs to the kth UE in the time resource τ_k, where $\mathcal{B}_a = \bigcup_{k \in \mathcal{U}} \mathcal{B}_k$. $\mathbf{w}_{kl} \in \mathbb{C}^{n_t}$ denotes the unit-norm precoding vector at AP l for UE k, ζ_{kl} is the transmitted message signal from AP l to UE k, and $\mathbb{E}[|\zeta_{kl}|^2] = 1$. q_{kl} denotes the transmit power, where the instantaneous transmit power of a single AP is assumed to be upper bounded by $q_{kl} \leq P_t$. We let $\mathbf{H}_{kl}$ denote the $n_r \times n_t$ channel matrix from AP l to UE k. The $n_r \times 1$ received signal vector at UE k becomes

$$\mathbf{y}_k = \sum_{l \in \mathcal{B}_k} \mathbf{H}_{kl} \mathbf{x}_{kl} + \mathbf{n}_k, \tag{3}$$

for $k = \{1, 2, \ldots, K\}$, where $\mathbf{n}_k \sim \mathcal{CN}(\mathbf{0}, N_0 \mathbf{I}_{n_r})$ is the noise vector at the receiver. $\mathcal{CN}(\mathbf{0}, \boldsymbol{C})$ denotes the circularly-symmetric complex Gaussian distribution with zero mean and covariance $\boldsymbol{C}$. $\mathbf{I}_{n_r}$ is the identity matrix of size n_r. We consider perfect knowledge of the channel coefficients at the APs and UEs considering the static nature of the IDS.

A. Coordinated Scheduling (CS)

In this cooperation strategy, only one AP-UE pair is active at a given time proportion. Therefore, the time proportion of UE k can be divided among APs as $\tau_k = \sum_{l \in \mathcal{B}_k} \tau_{kl}$. In this case, there will be no interference between UEs or APs. We replace $\mathbf{y}_k$ with $\mathbf{y}_{kl}$ since only AP l serves to UE k in time proportion τ_{kl}. In this case, in τ_{kl}, UE k receives

$$\mathbf{y}_{kl} = \mathbf{H}_{kl} \mathbf{x}_{kl} + \mathbf{n}_k, \tag{4}$$

where $l \in \{1, \ldots, L_a\}$ is the index of the AP transmitting in τ_{kl}. The SNR from AP l to UE k is

$$\mathrm{SNR}_{kl} = \frac{q_{kl} |\mathbf{v}_{kl}^H \mathbf{H}_{kl} \mathbf{w}_{kl}|^2}{W N_0}, \tag{5}$$

where $\mathbf{v}_{kl} \in \mathbb{C}^{n_r}$ is the unit-norm combining vector at the UE k for the received signal in τ_{kl}. We consider single data stream transmission from the AP to the selected UE. Due to the interference-free transmission, the optimal selection precoding and combining maximizes the SNR. To maximize the SNR, the precoder and combining vectors are chosen respectively as the dominant right and left singular vectors of the channel matrix $\mathbf{H}_{kl}$, where in [9], they are referred respectively as maximum ratio transmission (MRT) and maximum ratio combining (MRC). In this case the SNR becomes

$$\mathrm{SNR}_{kl} = \frac{q_{kl} \|\mathbf{H}_{kl}\|_2^2}{W N_0}, \tag{6}$$

where the singular value decomposition of the channel is $\mathbf{H}_{kl} = \mathbf{U}_{kl} \boldsymbol{\Sigma}_{kl} \mathbf{V}_{kl}^H$, and $[\boldsymbol{\Sigma}_{kl}]_{11} = \|\mathbf{H}_{kl}\|_2$. If several APs communicate orthogonally with UE k, the sum rate of UE k can be computed as

$$R_k = \sum_{l \in \mathcal{B}_a} \tau_{kl} W \log_2 \left(1 + \frac{P_t \|\mathbf{H}_{kl}\|_2^2}{W N_0}\right). \tag{7}$$

Due to the interference-free transmission, we set the $q_{kl} = P_t$, so that each AP can maximize its individual SNR level.

B. Non-Coherent Joint Transmission (NC-JT)

In NC-JT, multiple APs communicate with the same UE at the same time, but transmit independent data that needs to be decoded successively. In this case, all deployed APs will serve each UE jointly, $\mathcal{B}_k = \mathcal{B}_a$ for $k = \{1, \ldots, K\}$, and the received signal at user k in τ_k is

$$\mathbf{y}_k = \sum_{l \in \mathcal{B}_a} \mathbf{H}_{kl} \mathbf{x}_{kl} + \mathbf{n}_k. \tag{8}$$

If we consider the successive interference cancellation at the receiver, the rate at the UE can be computed as [10]

$$R_k = \tau_k W \log_2 \left(1 + \frac{\sum\limits_{l \in \mathcal{B}_a} q_{kl} |\mathbf{v}_{kl}^H \mathbf{H}_{kl} \mathbf{w}_{kl}|^2}{W N_0}\right), \tag{9}$$

from which the aggregated SNR can be identified as

$$\mathrm{SNR}_k = \frac{\sum\limits_{l\in\mathcal{B}_a} q_{kl}|\mathbf{v}_{kl}^H\mathbf{H}_{kl}\mathbf{w}_{kl}|^2}{WN_0}. \tag{10}$$

Similar to the orthogonal transmission case, the SNR is maximized by using MRT/MRC and maximum transmission power at each AP, which results in the rate at the receiver k becoming

$$R_k = \tau_k W \log_2\left(1 + \frac{P_t \sum\limits_{l\in\mathcal{B}_a} \|\mathbf{H}_{kl}\|_2^2}{WN_0}\right). \tag{11}$$

C. Coherent Joint Transmission (C-JT)

In coherent joint transmission, L_A APs transmit to a single UE jointly with phase synchronization. The optimum strategy in C-JT is to transmit the same message signal in a synchronous manner. In this case, $\mathcal{B}_k = \mathcal{B}_a$ for $k = \{1, \ldots, K\}$. The resulting received signal at UE k is

$$y_k = \sum_{l\in\mathcal{B}_a} \mathbf{H}_{kl}\mathbf{x}_{kl} + n_k, \tag{12}$$

where $\zeta_{kl} = \zeta_k$ for all $l \in \mathcal{B}_a$. The SNR can be represented by

$$\mathrm{SNR}_k = \frac{\left|\mathbf{v}_k^H\left(\sum\limits_{l=1}^{L_A}\sqrt{q_{kl}}\mathbf{H}_{kl}\mathbf{w}_{kl}\right)\right|^2}{WN_0}. \tag{13}$$

Considering the local precoding at the APs, we assume $\mathbf{w}_{kl}$ is the dominant right singular vector of $\mathbf{H}_{kl}$, where $[\mathbf{w}_{kl}]_i = [\mathbf{V}_{kl}]_{i1}$, for $i = 1, 2, \ldots, n_t$. To compute the combining vector, let us concatenate the channel matrices from the APs into a single channel matrix as $\mathbf{H}_k = [\mathbf{H}_{k1}, \mathbf{H}_{k2}, \ldots, \mathbf{H}_{kL_A}]$, and $\mathbf{w}_k = \left[\mathbf{w}_{k1}^T, \mathbf{w}_{k2}^T, \ldots, \mathbf{w}_{kL_A}^T\right]^T$. In this case, the SNR is maximized by $\mathbf{v}_k = \frac{\mathbf{H}_k\mathbf{w}_k}{\|\mathbf{H}_k\mathbf{w}_k\|}$, and the SNR at UE k becomes

$$\mathrm{SNR}_k = \frac{P_t\left|\mathbf{w}_k^H\mathbf{H}_k^H\mathbf{H}_k\mathbf{w}_k\right|^2}{WN_0}, \tag{14}$$

where we set $q_{kl} = P_t$ to maximize the SNR. The rate at UE k becomes

$$R_k = \tau_k W \log_2\left(1 + \frac{P_t\left|\mathbf{w}_k^H\mathbf{H}_k^H\mathbf{H}_k\mathbf{w}_k\right|^2}{WN_0}\right). \tag{15}$$

In the following section, we use (7), (11), and (15) to describe the rate requirement constraint of UEs in the AP deployment optimization problems.

III. Optimal Network Deployment

The main goal of this paper is optimal joint AP placement and resource allocation while guaranteeing certain data rates for all UEs. In the most general form, the problem that we consider can be stated as

$$\begin{aligned}
\textbf{P1:}\ &\text{minimize}_{\{\mathcal{B}_a,\tau_k\}}|\mathcal{B}_a| \\
&\text{C1: } R_k \geq \overline{R}_k, \forall k \in \mathcal{U} \\
&\text{C2: } \sum_{k=1}^{K}\tau_k = 1 \\
&\text{C3: } \mathcal{B}_a \subseteq \mathcal{B}.
\end{aligned} \tag{16}$$

The objective function in **P1** corresponds to the minimization of the number of deployed APs. C1 is the minimum rate condition for each user that needs to be satisfied, where the rate threshold for UE k is denoted by $\bar{R}_k$. C2 ensures that the time proportions assigned to the users are practically feasible. C3 mandates to select the APs from the subset of available locations for the APs to be deployed. In the following, we utilize several simplifications to efficiently solve **P1** considering the different transmission schemes.

A. Coordinated Scheduling

Let $\mathbf{a} = [a_1, a_2, \ldots, a_L]^T \in \{0,1\}^L$ denotes the deployment decision of the APs, where $a_l = 1$ if the AP is deployed at location B_l, and $a_l = 0$ otherwise. **P1** can be reformulated as

$$\begin{aligned}
\textbf{P2}:\ &\text{minimize}_{\{\mathbf{a},\tau_{kl}\}}\|\mathbf{a}\|_1 \\
&\text{C1: } \sum_{l=1}^{L}\tau_{kl}W\log_2\left(1 + \frac{P_t\|\mathbf{H}_{kl}\|_2^2}{WN_0}\right) \geq \overline{R}_k, \forall k \\
&\text{C2: } \sum_{l=1}^{L}\sum_{k=1}^{K}\tau_{kl} = 1 \\
&\text{C3: } \sum_{k=1}^{K}\tau_{kl} \leq a_l, \forall l \\
&\text{C4: } a_l \in \{0,1\}, \forall l.
\end{aligned} \tag{17}$$

C3 enforces the undeployed APs not to use time resources and thus we can remove the quadratic term in C1. As a result, **P2** is a mixed-binary linear programming problem, which has a convex structure except for the binary constraint in C4. Hence, the global optimum solution is obtained by the branch-and-bound algorithm [11]. This is still an NP hard mixed-integer problem that can only be solved in small-sized deployment scenarios. However, due to the static design of the deployment problem, time complexity with limited number of access points is tolerable.

B. Non-Coherent Joint Transmission (NC-JT)

In NC-JT, we consider τ_k instead of τ_{kl}, and use the deployment vector, $\mathbf{a}$, to formulate the deployment optimization

problem as

$$\begin{aligned}\textbf{P3}\text{: minimize}_{\{\mathbf{a},\tau_k\}}\ &\|\mathbf{a}\|_1\\ \text{C1: } &\tau_k W \log_2\left(1+\frac{P_t\sum_{l=1}^{L} a_l\|\mathbf{H}_{kl}\|_2^2}{WN_0}\right)\geq \bar{R}_k, \forall k\\ \text{C2: } &\sum_{k=1}^{K}\tau_k = 1\\ \text{C3: } &a_l\in\{0,1\}, \forall l.\end{aligned} \tag{18}$$

This is a mixed-binary non-convex quadratic programming problem due to C1 and C3. To remove the quadratic relation in C1, we can replace τ_k with $\tilde{\tau}_k = \tau_k^{-1}$, and the problem becomes

$$\begin{aligned}\textbf{P3}_{\text{alter-1}}\text{: minimize}_{\{\mathbf{a},\tau_k\}}\ &\|\mathbf{a}\|_1\\ \text{C1: } &\log_2\left(1+\frac{P_t\sum_{l=1}^{L} a_l\|\mathbf{H}_{kl}\|_2^2}{WN_0}\right)-\frac{\tilde{\tau}_k\bar{R}_k}{W}\geq 0.\\ \text{C2: } &\sum_{k=1}^{K}\frac{1}{\tilde{\tau}_k} = 1\\ \text{C3: } &a_l\in\{0,1\}, \forall l\end{aligned} \tag{19}$$

In this case, although C1 does not violate convexity, C2 becomes quadratic. To further simplify the problem, we can define $u_k \geq \frac{1}{\tilde{\tau}_k}$, such that

$$\left\|\begin{matrix}u_k\\ \tilde{\tau}_k\\ \sqrt{2}\end{matrix}\right\| \leq u_k+\tilde{\tau}_k. \tag{20}$$

This equation can be included as a new constraint since it is in a convex form. By replacing $\tilde{\tau}_k$ with u_k in C2 and relaxing the equality condition, and including (20), we can transform the optimization problem into a mixed-binary exponential cone program with a convex structure:

$$\begin{aligned}\textbf{P3}_{\text{alter-2}}\text{: minimize}_{\{\mathbf{a},\tilde{\tau}_k,u_k\}}\ &\|\mathbf{a}\|_1\\ \text{C1: } &\log_2\left(1+\frac{P_t\sum_{l=1}^{L} a_l\|\mathbf{H}_{kl}\|_2^2}{WN_0}\right)-\frac{\tilde{\tau}_k\bar{R}_k}{W}\leq 0, \forall k\\ \text{C2: } &\sum_{k=1}^{K}u_k \leq 1\\ \text{C3: } &a_l\in\{0,1\}, \forall l\\ \text{C4: } &\left\|\begin{matrix}u_k\\ \tilde{\tau}_k\\ \sqrt{2}\end{matrix}\right\| \leq u_k+\tilde{\tau}_k, \forall k.\end{aligned} \tag{21}$$

Solving $\textbf{P3}_{\text{alter-2}}$ using the branch and bound algorithm has similar time complexity as solving **P2**.

C. Coherent Joint Transmission (C-JT)

The SNR expression of C-JT in (13) can be rewritten using the entries of the deployment vector $\mathbf{a}$ as

$$\text{SNR}_k = \frac{P_t\left|\left(\mathbf{v}_k^H\sum_{l=1}^{L} a_l\mathbf{H}_{kl}\mathbf{w}_{kl}\right)\right|^2}{WN_0}. \tag{22}$$

This expression cannot be directly utilized for optimization due to several reasons. One is that the optimal combining vector depends on the binary deployment vector and the local channel matrices. The other is that the resulting SNR would have binary quadratic terms, which must be simplified further. If we define $\mathbf{b}_k = \sum_{l=1}^{L_A} a_l\mathbf{H}_{kl}\mathbf{w}_{kl}$, the optimal combining vector is $\mathbf{v}_k = \frac{\mathbf{b}_k}{\|\mathbf{b}_k\|}$. The resulting SNR of UE k is

$$\text{SNR}_k = \frac{P_t\|\mathbf{b}_k\|_2^2}{WN_0}. \tag{23}$$

We define $\mathbf{m}_{kl} = \mathbf{H}_{kl}\mathbf{w}_{kl} \in \mathbb{C}^{n_r}$ and $\mathbf{M}_k = [\mathbf{m}_{k1}, \mathbf{m}_{k2}, \ldots, \mathbf{m}_{kL}] \in \mathbb{C}^{n_r\times L}$. We can then model $\|\mathbf{b}_k\|^2$ as

$$\|\mathbf{b}_k\|^2 = \bar{\mathbf{m}}_k^T\,\text{vec}\,(\mathbf{Z}), \tag{24}$$

where $\bar{\mathbf{m}}_k = \text{vec}\left(\text{Re}\left\{\mathbf{M}_k^H\mathbf{M}_k\right\}\right)$. vec$(\cdot)$ denotes the vectorization operation. We define a symmetric binary matrix, $\mathbf{Z} = \mathbf{a}\mathbf{a}^T \in \{0,1\}^{L\times L}$ and $[\mathbf{Z}]_{ij} = z_{ij} = a_i a_j$. The diagonal elements of the matrix can be replaced by a_i. The off-diagonal elements of the matrix can be replaced by the following constraints [12]:

$$\begin{aligned}&0\leq z_{ij}\leq z_{jj},\\ &0\leq z_{ii}-z_{ij}\leq 1-z_{jj},\end{aligned} \tag{25}$$

where $z_{ii}, z_{jj}, z_{ij} \in \{0,1\}$. The simplified problem statement in **P3** can be utilized here by transforming $\mathbf{a}$ to $\mathbf{Z}$. The deployment optimization problem in the case of C-JT becomes

$$\begin{aligned}\textbf{P4:}\ \text{minimize}_{\{\mathbf{Z},\tilde{\tau}_k,u_k\}}\ &\text{Tr}(\mathbf{Z})\\ \text{C1: } &\log_2\left(1+\frac{P_t\bar{\mathbf{m}}_k^T\,\text{vec}\,(\mathbf{Z})}{WN_0}\right)-\frac{\tilde{\tau}_k\bar{R}_k}{W}\leq 0, \forall k\\ \text{C2: } &\sum_{k=1}^{K}u_k\leq 1\\ \text{C3: } &z_{ij}\in\{0,1\}, \forall i,j\\ \text{C4: } &\left\|\begin{matrix}u_k\\ \tilde{\tau}_k\\ \sqrt{2}\end{matrix}\right\| \leq u_k+\tilde{\tau}_k, \forall k\\ \text{C5: } &0\leq z_{ij}\leq z_{jj}, \forall i,j\\ \text{C6: } &0\leq z_{ii}-z_{ij}\leq 1-z_{jj}, \forall i,j.\end{aligned} \tag{26}$$

This is also a mixed-integer exponential cone programming problem, and the global optimum solution can be obtained by the branch-and-bound method.

IV. Numerical Analysis

In this section, we first detail our case study with RT simulations, and we provide the results of optimization problems presented in the previous section.

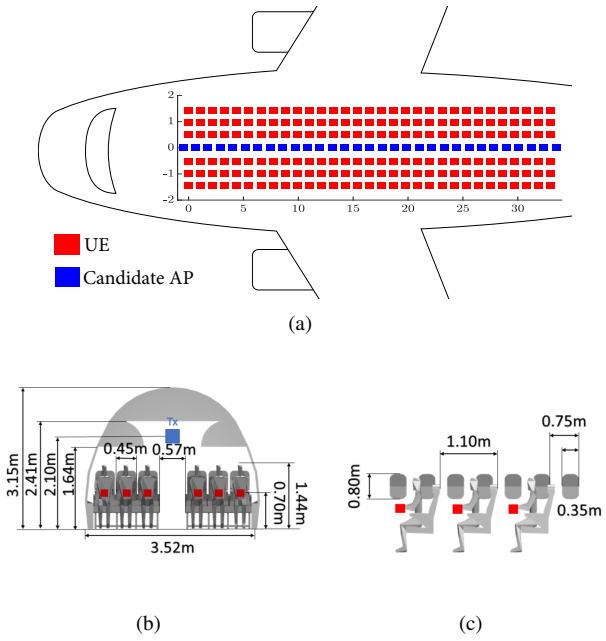

(a)

(b) (c)

Fig. 1. Airplane geometry in RT from (a) top, (b) front and (c) side views.

TABLE I
DIELECTRIC PROPERTIES OF MATERIALS AT 2.4 GHZ AND 28 GHZ.

Material	2.4 **GHz**		28 **GHz**		**Thickn.**
	ϵ	σ	ϵ	σ	(cm)
Skin [14]	19.3	30.40	13.8	37.60	0.1
ABS [15]	2.4	0.028	2.4	0.028	0.3
Nylon [16]	3.01	0.03	3.05	0.05	0.25
Glass [17]	6.27	0.15	6.27	0.40	0.3

TABLE II
SIMULATION PARAMETERS FOR THE RT.

Parameter	**Value**
# Candidate AP locations	31
# UEs	180
# AP antennas	64
# UE antennas	4
Array geometry (AP, UE)	ULA
Transmit power	27 dBm
Antenna gain (AP, UE)	0 dBi
UE noise figure	10 dB
Bandwidth	500 MHz / 50 MHz
Carrier frequency	28 GHz / 2.4 GHz
Antenna polarization	V-V (AP-UE)
Antenna type	Isotropic
Transmission line loss	0 dBm

A. RT Channel Simulations

We consider an airplane cabin scenario, where the fuselage is a dielectric material with a half-cylindrical shape. To obtain the channel coefficients from the candidate APs to the UEs, we use a commercial RT tool, Wireless Insite[1], which provides accurate channel modeling in complex environments by using the shooting-and-bouncing ray model. The RT model of an IDS environment with 30 rows of passenger seats (6 seats per row) and 31 candidate AP positions are shown in Fig. 1(a). The geometry of the RT environment is realistically captured from commercial airplane models, and detailed in Fig. 1(b) and Fig. 1(c). The APs are located 2.1 m above the floor and in the middle of the corridor. We consider two different frequency bands: 2.4 GHz and 28 GHz. For each passenger seat, we consider single UE at 0.7 m height and a total of 180 UE locations.

The dielectric parameters of the materials are given in Table I. The passenger seats are modeled by nylons. ABS is considered for the fuselage, which is a common material for aircraft bodies [8]. For the windows, we consider glass as the closest material. In this table, ϵ denotes the permittivity and σ denotes the conductivity. The material characteristics are obtained from several different measurement works considering the given frequency bands in their analyses. RT simulation parameters for the AP-UE nodes are given in Table II. Transmit power is determined by health regulations in short-range indoor close-by environments such as IDS [13].

B. Performance Evaluation

We evaluated the objective function values of **P2**, $\mathbf{P3}_{\text{alter-2}}$ and **P4** for different rate requirements and antenna configurations considering the mmWave network setup. The results are illustrated in Fig. 2. The data rate per UE is the rate requirement in the optimization problems denoted by $\bar{R}_k$, and assumed to be equal for all UEs. The deployed AP number is the optimal result obtained by solving the respective problem. Although, we consider data rates per UE as low as 1 Mbps, optimal AP number does not get smaller than three. This is due to the blockage limitation of the mmWave channels. Although the size of the environment is fairly small, a high number of objects and human bodies cause high levels of blockage (approximately 10 dB of loss per row, as detailed in [8]). Beyond the vertical limits, even deploying more APs do not improve the data rate of UEs since the SNR levels are already high and the system is limited by the available bandwidth. In Fig. 2(a), we can observe that at low data rates (42-44 and 46-49 Mbps), all cooperation strategies require the same number of APs. While C-JT and NC-JT have more time resources to utilize, the received signal levels are not high enough to provide the data rate for all UEs, and more APs are deployed to provide better coverage. CS cannot perform better than 53.3 Mbps even when activating more APs. Since in CS, the UEs are limited by a single AP link, they cannot gain more from the other APs. As the cooperation between the APs improves, the performance limit gets higher. In Fig. 2(b), NC-JT and C-JT perform better than in Fig. 2(a) due to higher beamforming gain from the APs.The considered system is limited by 68 Mbps even when we deploy APs to all candidate locations.

Table III provides a comparison between the two different frequency bands. The main difference is that at 2.4 GHz, the blockage is less effective but the bandwidth is 10 times less than at 28 GHz. As a result, we see that for a data rate threshold up until 4.3 Mbps, we can deploy 1 AP to cover the airplane cabin in 2.4 GHz band. Due to the wider bandwidth in

[1]Wireless InSite, available at: http://www.remcom.com/wireless-insite

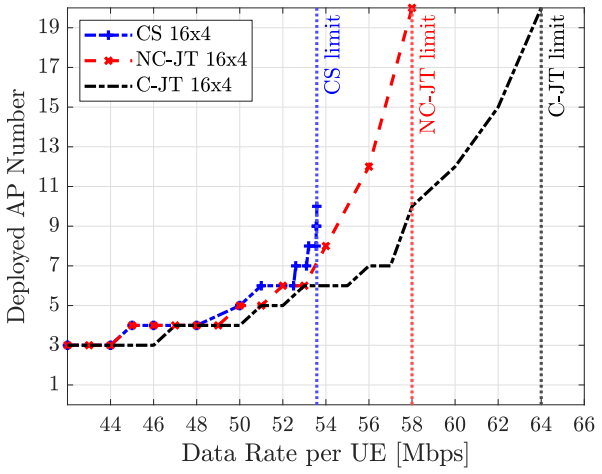

(a)

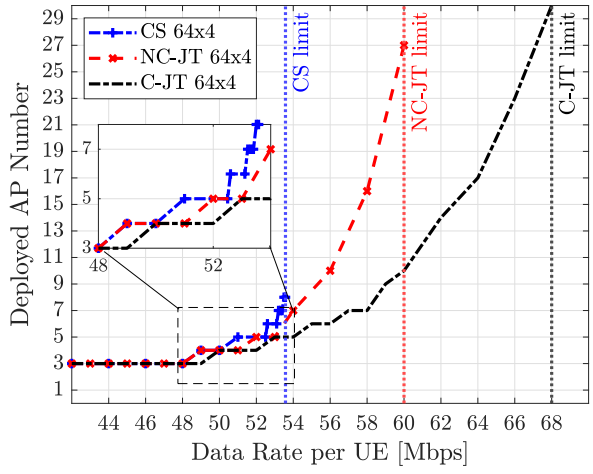

(b)

Fig. 2. Number of required APs vs the data rate threshold per UE for different cooperation strategies and antenna configurations for $n_t \times n_r$ is given by (a) 16×4 (b) 64×4.

TABLE III
MMWAVE AND SUB-6GHZ COMPARISON CONSIDERING C-JT WITH 64×4 ANTENNAS.

Deployed #AP	Data rate per UE	
	28 GHz	2.4 GHz
1	Infeasible	4.3 Mbps
3	49 Mbps	5.6 Mbps
5	54 Mbps	6.1 Mbps
15	63 Mbps	6.9 Mbps
28	68 Mbps	7.3 Mbps

mmWave, the data rates are almost 9 times higher than the 2.4 GHz, and exceed the requirements of emerging applications such as VR (30-60 Mbps for indoor applications [1]).

V. CONCLUSION

In this paper, we propose a framework for identifying the optimal AP deployment that minimizes the number of APs while satisfying the rate requirement of each user. We applied the framework to indoor channels, particularly a realistic airplane cabin environment simulated using a commercial RT program to obtain the channel coefficients in the 28 and 2.4 GHz bands. The numerical results demonstrate that at least 3 APs are required in the mmWave band to cover the environment due to the blockage effect. While the 2.4 GHz band has better channel conditions, the 10 times higher bandwidth in mmWave results in 9 times higher data rates per user. As future work, to fully harness the large available bandwidth, we plan to extend the proposed deployment considering multi-user MIMO algorithms with interference management.

REFERENCES

[1] Ericsson, "Ericsson Mobility Report, Mobile subscriptions Q2 2021," August 2021.

[2] G. R. Maccartney, T. S. Rappaport, S. Sun, and S. Deng, "Indoor office wideband Millimeter-Wave propagation measurements and channel models at 28 and 73 GHz for ultra-dense 5G wireless networks," *IEEE Access*, vol. 3, pp. 2388–2424, 2015.

[3] D. Maamari, N. Devroye, and D. Tuninetti, "Coverage in mmwave cellular networks with base station co-operation," *IEEE Transactions on Wireless Communications*, vol. 15, no. 4, pp. 2981–2994, 2016.

[4] N. Palizban, S. Szyszkowicz, and H. Yanikomeroglu, "Automation of millimeter wave network planning for outdoor coverage in dense urban areas using wall-mounted base stations," *IEEE Wireless Communications Letters*, vol. 6, no. 2, pp. 206–209, 2017.

[5] I. Mavromatis, A. Tassi, R. J. Piechocki, and A. Nix, "Efficient millimeter-wave infrastructure placement for city-scale its," in *2019 IEEE 89th Vehicular Technology Conference (VTC2019-Spring)*, 2019, pp. 1–5.

[6] Y. Liu, Y. Jian, R. Sivakumar, and D. M. Blough, "Maximizing line-of-sight coverage for mmwave wireless LANs with multiple access points," *IEEE/ACM Transactions on Networking*, vol. 30, no. 2, pp. 698–716, 2022.

[7] S. Chatterjee, M. J. Abdel-Rahman, and A. B. MacKenzie, "A joint optimization framework for network deployment and adaptive user assignment in indoor millimeter wave networks," *IEEE Transactions on Wireless Communications*, vol. 20, no. 11, pp. 7538–7554, 2021.

[8] O. A. Topal, M. Ozger, D. Schupke, E. Björnson, and C. Cavdar, "mmWave communications for indoor dense spaces: Ray-tracing based channel characterization and performance comparison," in *International Conference on Communications*, 2022, pp. 516–521.

[9] D. Love and R. Heath, "Equal gain transmission in multiple-input multiple-output wireless systems," *IEEE Transactions on Communications*, vol. 51, no. 7, pp. 1102–1110, 2003.

[10] R. Tanbourgi, S. Singh, J. G. Andrews, and F. K. Jondral, "A tractable model for noncoherent joint-transmission base station cooperation," *IEEE Transactions on Wireless Communications*, vol. 13, no. 9, pp. 4959–4973, 2014.

[11] Gurobi optimizer reference manual. Gurobi Optimization, LLC. Accessed: Oct. 2022. [Online]. Available: https://www.gurobi.com

[12] W. Wei and J. Wang, *Modeling and optimization of interdependent energy infrastructures*. Springer, 2020.

[13] I. C. on Non-Ionizing Radiation Protection, "Guidelines for limiting exposure to time-varying electric, magnetic, and electromagnetic fields (up to 300 Ghz)," *Health physics*, vol. 74, no. 4, pp. 494–522, 1998.

[14] T. Wu, T. S. Rappaport, and C. M. Collins, "The human body and millimeter-wave wireless communication systems: Interactions and implications," in *International Conf. on Commun.*, 2015, pp. 2423–2429.

[15] R. Singh, G. S. Sandhu, R. Penna, and I. Farina, "Investigations for thermal and electrical conductivity of ABS-Graphene blended prototypes," *Materials*, vol. 10, no. 8, 2017.

[16] B. Riddle, J. Baker-Jarvis, and J. Krupka, "Complex permittivity measurements of common plastics over variable temperatures," *IEEE Trans. Microw. Theory Techn.*, vol. 51, no. 3, pp. 727–733, 2003.

[17] I. T. U. Recs., "Propagation data and prediction methods for the planning of indoor radio communication systems and radio local area networks in the frequency range 900 MHz to 100 GHz," 2012, Geneva, Switzerland.